Mining, Metallurgy & Exploration (2025) 42:45–59
https://doi.org/10.1007/s42461-024-01148-2

An Insight into Limestone Pillar Stability in Dipping Environments Using Actual Mine Geometries

Gamal Rashed[1] · Brent Slaker[1] · Nicole Evanek[1]

Received: 3 September 2024 / Accepted: 21 November 2024 / Published online: 7 January 2025

Abstract
As stone mine operations continue to develop in more challenging conditions including inclined seams, more complex loading conditions and pillar geometries are generated. The main objective of this study is to gain more understanding about the effect of seam inclination on the strength, the loading path, deformation of sidewalls, and yield patterns of a stone pillar using numerical models. The modeled width-to-height (W/H) ratio of the pillars, the unconfined compressive strength of limestone material, in situ stress field, and roof interface were varied to consider their potential distribution across underground limestone mines in the United States. Two actual mine geometries, referred to as a-type and b-type, were modeled. In a-type mine geometry, the roof is dipping while the floor is flat, making one side of the pillar shorter than the other side. In b-type mine geometry, the roof and floor lines of pillars are dipping while the headings/crosscuts are flat. The intention is not to compare pillar stability in these mine geometries, but to show pillar response in different dipping environments because these environments are different in pillar size, shape, and extraction ratio. Numerical modeling results indicate that dip pillars have reduced strength compared to flat pillars. The shear strength between the pillar and the surrounding rock has an impact on dipping pillar response. Dipping pillars experience high shear stresses, highly non-uniform stress distributions, and asymmetric yield pattern with more yielding compared to flat pillars. All these reasons place dipping pillars, particularly those with a small width-to-height ratio (<1) at an elevated risk of instability. The yield pattern for a flat pillar is simple while it is complex for a dipping pillar and depends on numerous parameters such as the width-to-height ratio of the pillar and seam inclination. The down-dip side of dipping pillars experiences more outward normal displacement compared to the up-dip side, while it experiences less vertical displacement. The results of this study improve the understanding of pillar stability in dipping environments and advance the ultimate goal of reducing the risk of dipping pillar instability in underground stone mines.

Keywords Underground stone pillar · Seam inclination · Pillar strength · Dip pillar

1 Introduction

There are currently 101 active underground stone mines in the United States [18]. These mines typically use a room-and-pillar mining method, and some mines are forced to operate in inclined deposits or contain individual sections of a mine which may be inclined. Dipping mines tend to be located along synclinal or anticlinal structures with dips between 5 and 20°, but there are cases of dips in excess of 20° [4]. Dougherty reported that in a subsample of the industry, approximately 10% of active underground stone mines in the United States claimed to have dips in excess of 3° [2]. The effect of this dip on the support performance of pillars has not been thoroughly studied and is part of an ongoing research project by the National Institute for Occupational Safety and Health (NIOSH) to understand stone pillar stability in challenging mining environments. The purpose of this paper will be to explore the effect of seam inclination on pillar stability through numerical modeling using actual mine geometries. Many researchers simplified the actual mine geometry to investigate the stability of dipping pillars using analytical or numerical methods [12, 15, 17, 21, 23, 26]. However, simplifying the geometry of dipping pillars may introduce unrealistic deformation and rock failure responses [23].

✉ Gamal Rashed
mqx3@cdc.gov

[1] CDC/NIOSH/PMRD, Pittsburgh, Pennsylvania, USA

Empirical pillar strength equations for pillar stability [5], [24], [16], [27], [13], [1], [25] having an underlying database often include dipping deposits, and it is the experience of the authors that many of these relationships are applied to the design of dipping pillars, but they do not explicitly consider the unique loading conditions experienced in a dipping pillar differently than they do a flat-lying pillar.

Pritchard and Hedley 22 described observations of progressive pillar failures at the dipping Denison Mine and created a classification scheme. The asymmetrical pillar deterioration shown in Pritchard and Headley's scheme leads to the discussion presented in this paper. This study aims to examine the impact of multiple parameters, such as seam inclination, pillar width-to-height ratio, in situ stress conditions, and pillar shape on dip-pillar stability using actual mine geometries. Every permutation of pillar geometries and loading conditions cannot possibly be considered, but a range of common situations and conditions are considered to highlight potential areas of concern when evaluating or designing pillars in dipping environments.

2 Pillar Geometry in Dipping Environment

There are several ways in which the shape and size of a pillar are both inherently and necessarily different in dipping room-and-pillar hard rock mines. Operationally, the dip of the deposit presents a few challenges for equipment and pillar design. Several geometries are given as examples of a common means of dealing with a dipping limestone deposit, shown in Figure 1. These are not suggestions for how to mine various dips, but combinations or deviations from these examples are certainly possible.

In considering Figure 1A, there is no dip, and the classic understanding of pillar stability should apply. When the geometry shown in Figure 1B and Figure 2 is considered, the applicability of past pillar stability research comes into question. It is generally preferred to not work on a steeply sloping ground, and as a result, the headings, assumed to be along the strike in this example, will likely be approximately level from rib-to-rib along the floor. In a dipping deposit, this will necessitate a crosscut floor that dips more steeply than the deposit itself, and if dips become too steep for equipment to traverse, angled crosscuts may be required to reduce the slope of the roadway, creating rhomboidal pillars, as described in Murphy et al. 19. Rhomboidal pillars fall outside the scope of this study, but special attention should still be given to acute angles formed on pillar corners and potential implications on intersection width. This dipping geometry also creates a differential height across the pillar where there is a short side, H_S, and a tall side, H, to the pillar. The width, W_{AD}, of the pillar is simply shown to contrast a width parallel to the dip of the deposit. There is some inconsistency in the literature and in how pillar widths are reported when the deposit dips, but in the belief of the authors, this "shortest distance" width is most likely to be projected on a mine map and is often more relevant for discussing pillar stability, and as such will be what is meant in this paper when the term "pillar width" is used. Lastly, the geometry shown in Figure 1C may be found in situations where the dip is too steep for dipping crosscuts and possibly too steep to mine the roof along the bedding. At these steep dips, regardless of how the roof is mined, there is still an issue of highly offset ribs that are distinctly dissimilar to the flat-lying pillars. The pillar heights, H_{BC} and H, are unlikely to be appropriate substitutes for effective height in a pillar strength equation. In this study, the pillar geometries shown in Figure IB and IC are referred to as the a-type and b-type pillars, respectively.

3 The Study Parameters

In this study, FLAC3D models were used to evaluate the impact of numerous parameters expected to influence the stability of stone pillars in dipping environments. The study parameters are as follows:

1. Two actual mine geometries have been simulated, a-type and b-type geometries, shown in Figure 1. They are also shown in Figure 4 in the Section 5 below.
2. The modeled stone pillar W/H ratio varied from around 0.5 to 3.0. For a-type geometry, an average pillar height for the short (up-dip) side and the tall (down-dip) side of the pillar was used to calculate the W/H ratio. For b-type geometry, the up-dip and down-dip sides of the pillar are equal.
3. Seam inclination varied from 0° to 20° at 10° increments for a-type geometry, and operational constraints would likely preclude the creation of a-type pillars in dips exceeding 20°. On the other hand, for b-type geometry, seam inclination varied from 0° to 40° at 10° increments.
4. In situ stresses were varied to consider low and high horizontal stress environments. The horizontal/vertical stress ratios (*k*-ratio) utilized in this study are 0.3 and 3.0.
5. Two conditions for roof-pillar interface shear strengths (weak and strong) have been explored. The shear strength for a weak interface is smaller than that of the limestone material. However, the shear strength for a strong interface condition is as strong as the limestone material.
6. Two intact rock strengths were used, with the unconfined compressive strength (UCS) of 80 MPa and 150 MPa to simulate moderate and strong limestone strengths. The definition of moderate and strong strengths in this study does not follow any of the current classification systems.
7. Square pillar shapes have been modeled. Pillar size refers to the projected dimension on a mine map.

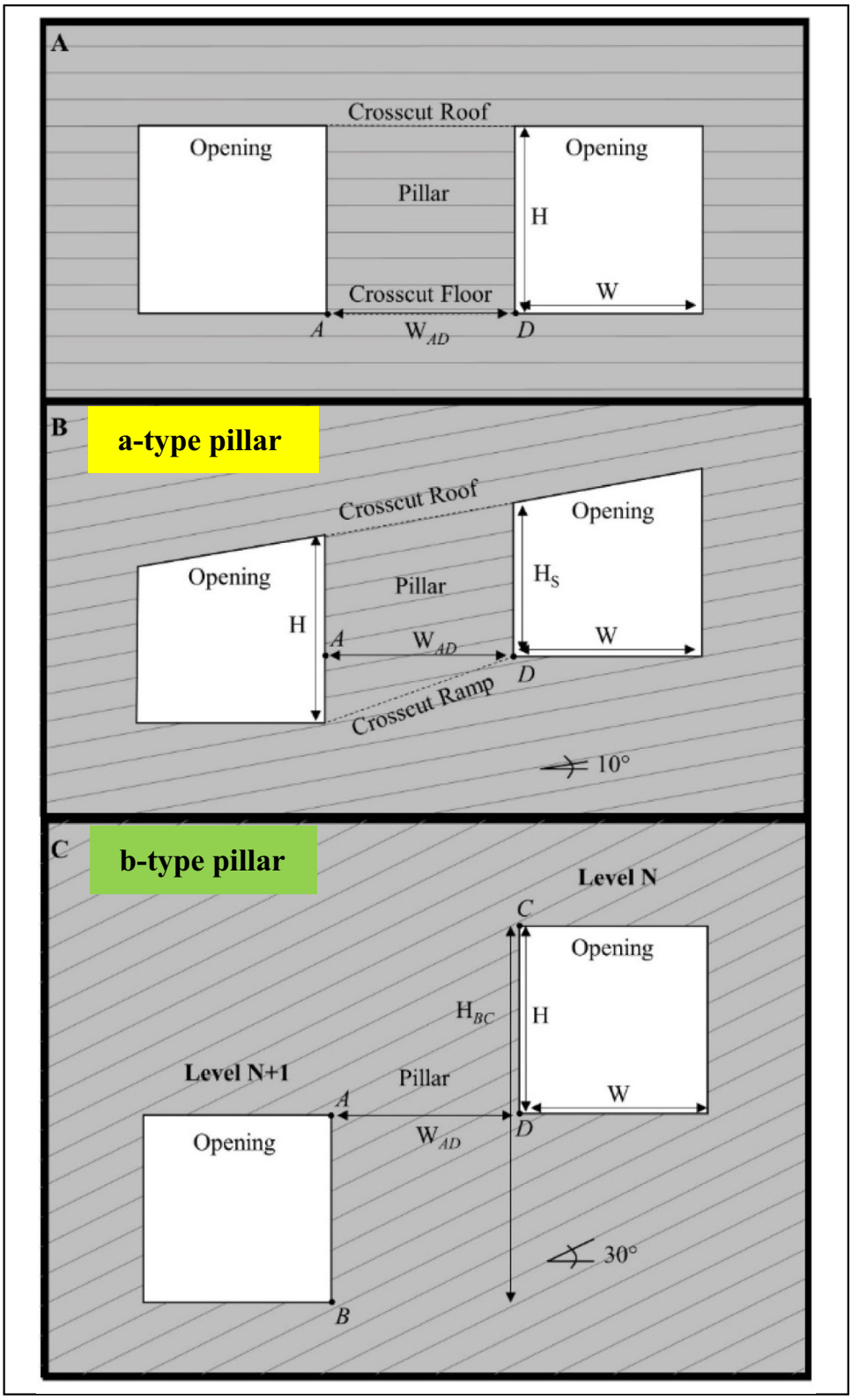

Fig. 1 Schematic for dipping versus flat mine geometry

8. The extraction ratio for square pillars of the a-type is about 0.67 (pillar width = 20 m and entry/crosscut width = 14 m), while it is about 0.60 for the b-type geometry (pillar width = 24 m and entry/crosscut = 14 m).

4 Model Calibration

Numerical models are a reliable tool to gain more insight about stone pillar stability if they are calibrated. FLAC3D

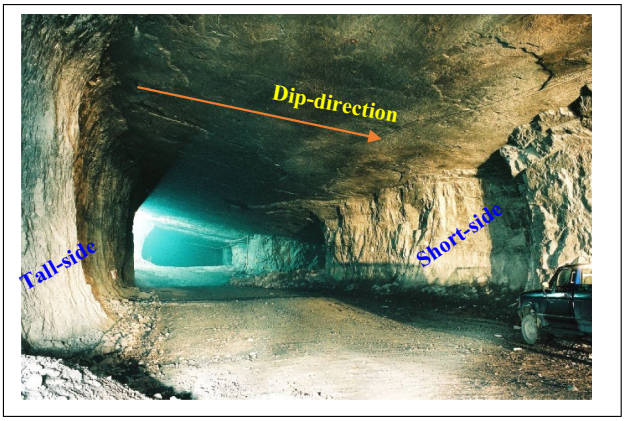

Fig. 2 An example of the a-type pillar from an underground limestone mine

models were calibrated using empirical pillar strength equations (see Figure 3). The pillars in the calibrated models have a square cross-sectional area of 20 m × 20 m (65.5 ft × 65.5 ft) based on surveyed data. To change the W/H ratio of a pillar, the pillar width was fixed while the height of the pillar was adjusted. The calibrated stone pillars have an element size of 0.5 m (1.64 ft). The roof and the floor material were simulated using an elastic material model, and they were assumed to be limestone as well. The intact rock properties for the medium and strong limestone material used in this paper are shown in Table 1.

The Hoek-Brown failure criterion was utilized to model the peak strength of the limestone pillars [7]. The jointed rock mass was modeled through selecting the appropriate geological strength index (GSI). A peak GSI of 75 was chosen to represent an undisturbed limestone rock mass and a disturbance factor of zero due to blasting was assumed. To simulate a softening of the limestone material after the peak strength was reached, a residual value for the GSI of 10 was assumed based on the calibration. The rock mass modulus for the modeled limestone pillars was estimated [8]. Figure 3 shows a comparison between the empirical pillar strength equations and the FLAC3D models of a flat-lying pillar of intact rock strength = 150 MPa. The strength of the stone pillars predicted from the FLAC3D model is roughly in the middle of an imaginary upper and lower bound for all empirical pillar strength equations.

Table 1 Summary of laboratory test results for the limestone properties used in this study

Parameter	Value
UCS, MPa	80 and 150
Poisson's ratio (v)	0.25
Young's modulus (E_i), MPa	50,800 and 70,800*
Hoek-Brown m_i parameter	9.98

*Young's modulus for medium and strong limestone in this study

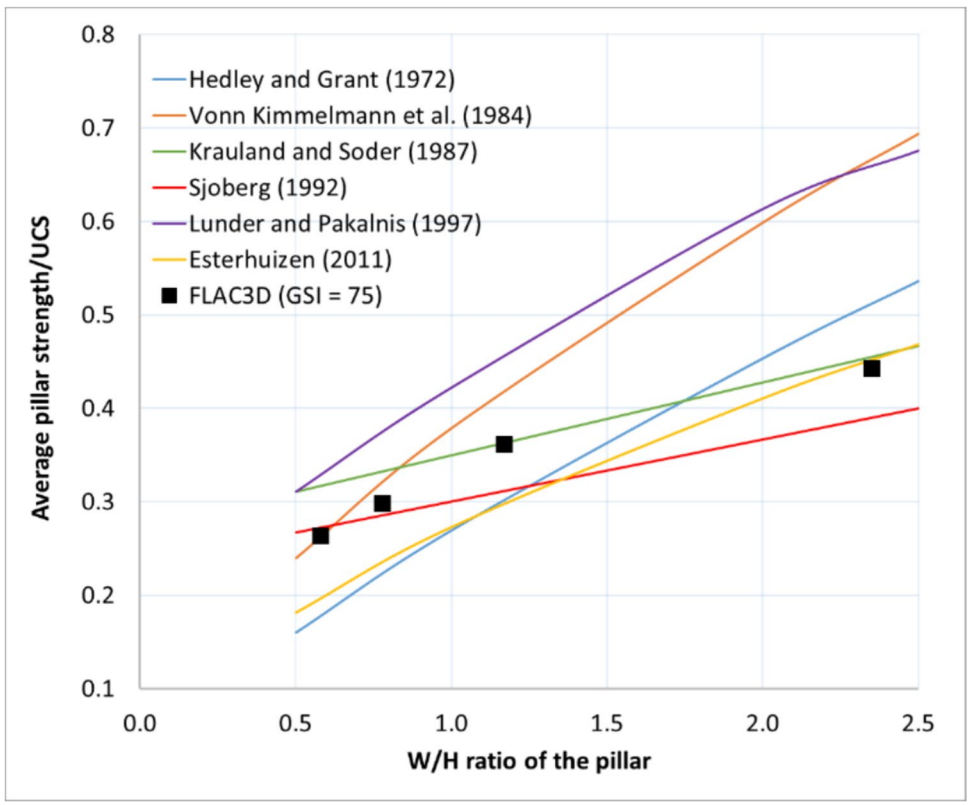

Fig. 3 Comparing the empirical pillar strength equations with FLAC3D model results

5 Model Setup

To investigate the impact of seam inclination on stone pillar stability in dipping environments, a 5×5 array of pillars rather than one pillar was generated to keep the roller boundary conditions far from the study pillar (colored in red and located in the middle of the array) and to reduce the error in the average pillar strength according to Martin and Maybee 17. A schematic of the a-type and b-type geometries in FLAC3D is shown in Figure 4. The axial load capacity of the modeled stone pillar was estimated by averaging vertical stress (σv) for all elements at mid-pillar height along the blue dash line shown in Figure 4.

The total thickness of the roof layer is three times the pillar height. The thickness of the roof is equivalent to the thickness of the floor. An elastic material model was assigned for both the roof and the floor, while the Hoek-Brown material model was adopted for the modeled pillars. The same extraction ratio was assumed for all models of the same mine geometry; the extracted area is measured in the plan view of the seam. Hence, a valid comparison for average pillar strength can be obtained at various W/H ratios and dip angles.

A potential sliding or separation at the roofline can be modeled using a weak roof interface between stone pillars and the roof. Jaeger et al. [11] measured coefficients of friction between sliding rock surfaces and found values between 0.5 and 0.9. A coefficient of friction of 0.5 was used in this study to replicate a weak roof/pillar interface. However, to simulate a strong interface, the roof and the modeled pillars were attached such that neither sliding nor separation was allowed. For a-type pillars, the FLAC3D models were solved with weak and strong roof/pillar interfaces. The weak interface properties used in the FLAC3D models are illustrated in Table 2. For b-type pillars, only an attached or strong roof/pillar interface condition has been modeled because of the FLAC3D limitation to simulate stair-steps interfaces. The floor is attached to pillars in all a-type and b-type models.

The numerical model was solved in three steps: (1) geostatic, the in situ stresses are initialized; the study pillar is at a depth of cover equal to 183 m (600 ft); (2) development, all headings and crosscuts are extracted. The cutting sequence was not considered in this study, the "zone relax excavate" command in FLAC3D was used to extract the material to minimize unrealistic yield in headings/crosscuts [10],(3) displacement loading, the roof was moved at 0.5E−6 m/cycle to fail the study pillar.

6 6- Model Results and Discussion

The main goal of this study is to utilize FLAC3D models to gain more insight into the impact of seam inclination on stone pillar stability using actual—not simplified—pillar

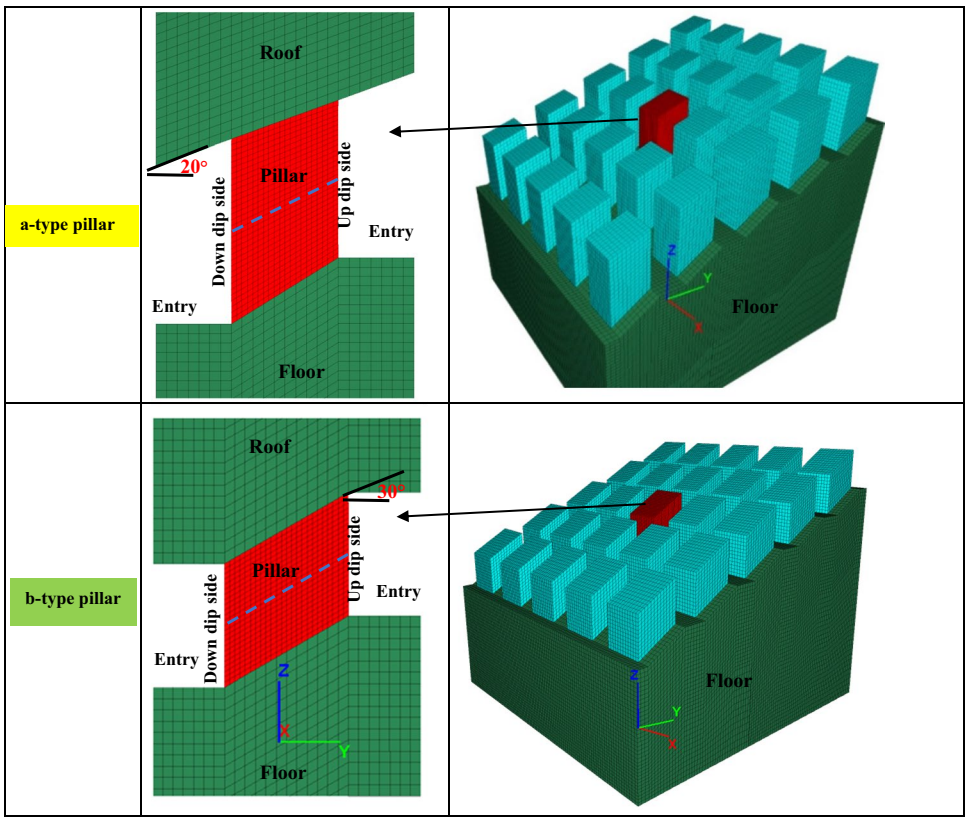

Fig. 4 Schematic for the 5×5 array of pillars for the a-type and b-type mine geometries with zoom-in at the study pillar colored in red in the middle of the array

Table 2 Roof-pillar interface properties used in the a-type pillar geometry [23]

Parameter	Value
Normal stiffness (*kn*), MPa/m	13,000
Shear stiffness (*ks*), MPa/m	2600
Friction angle (φ), degree	25.0
Friction-residual ($\varphi\prime$), degree	14.0
Cohesion (c), MPa	1.0
Cohesion-residual ($c\prime$), MPa	0.35
Tension (σ_t), MPa	0.20
Tension-residual ($\sigma_t\prime$), MPa	0.07

geometry and how seam inclination creates asymmetric loading path, uneven deformation at the opposite sidewalls, asymmetric yielding pattern, and a reduction in the average pillar strength. Please note that in this study the no and 0° dipping pillar are used interchangeably.

7 Effect of Seam Inclination on Loading Path

A pillar loaded by an inclined seam is subjected to an oblique loading (compressive and shear loads), while the pillar is loaded axially when the seam is flat. Pillars subjected to both compressive and shear stresses behave differently from those subjected to pure compression [26]. The results of this study suggest that the loading path/mechanism is always looking for the stiffest, shortest direction to transfer the overburden load from roof-to-pillar-to-floor. Figure 5 shows the major principal stress redistribution at the development loading stage for the a-type pillar, b-type pillar, and flat pillar. The *k*-ratio is 3. Seam inclination can have a significant effect on the intensity and reorientation of the principal stresses. The intensity of the induced stress is higher for dipping pillars than for flat pillars, although the magnitude of the in situ stresses is the same. For dipping pillars, there is a preferred orientation for the loading path, which is inclined with respect to the centerline of the pillar. Multiple factors can control that loading path, among which are the dip angle, the W/H ratio of the pillar, and the mine geometry.

For the a-type and b-type pillars, when the W/H ratio of the pillar is small (less than 1.0), the loading path takes the short diagonal and may pass through the pillar core (see Figure 5). On the other hand, for pillars with a large W/H ratio, the loading path is inclined with respect to the vertical axis of the pillar, but it does not go through the pillar core. For small dip angles (10° or less) and large W/H ratios (such as 3.0), the loading path was not different from a flat pillar. For flat pillars, the loading path is always vertical and parallel to the centerline of the pillar, irrespective of the W/H ratio of the pillar (see Figure 5b). Pritchard and Hedley 22 found that the failure in pillars at the Denison Mine was oriented such that it corresponded with the angle of the principal stress relative to the pillars.

8 Effect of Seam Inclination on Axial Pillar Strength

Numerical models can be used to gain more insight about the impact of seam inclination on axial pillar strength. The axial pillar strength was estimated by averaging the vertical

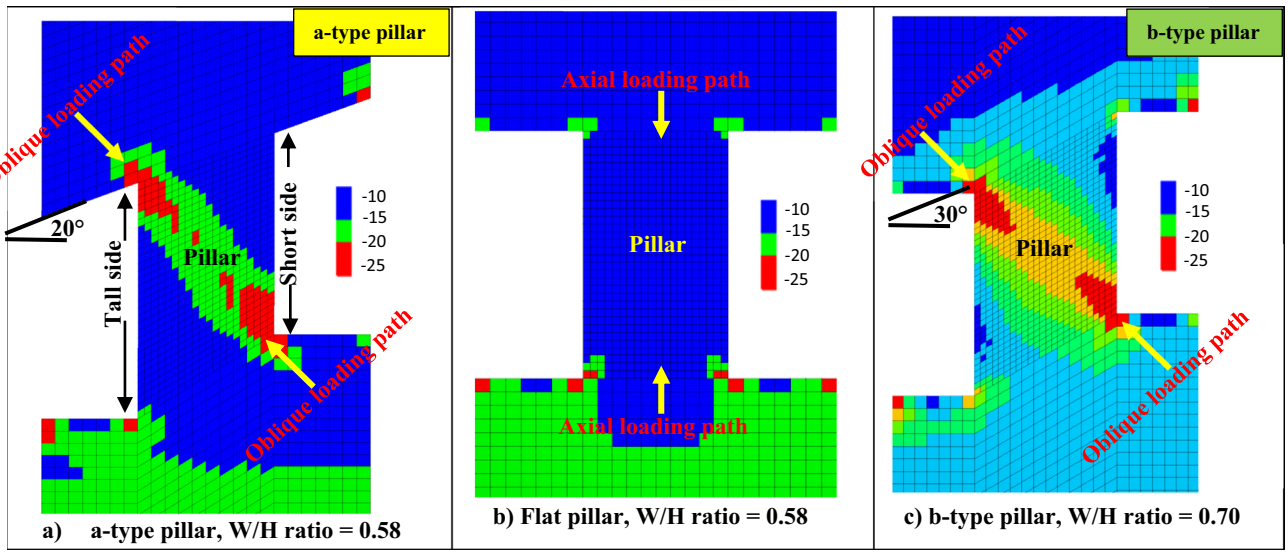

Fig. 5 Major principal stress distribution at mid-pillar length for the **a** a-type pillar, **b** flat pillar, and **c** b-type pillar; *k*-ratio = 3.0, similar patterns were observed in *k*-ratio = 0.3; stress units are in MPa. Negative values mean compression

stress for all elements at the mid-height of the pillar. Figure 6 shows the axial pillar strength of the a-type pillar at various seam-inclinations and W/H ratios for two intact rock strengths (80 MPa and 150 MPa) with *k*-ratio = 3.0. The pillars have a square projected cross-sectional area (20 m × 20 m) and a weak roof/pillar interface. The estimated pillar strength was normalized by dividing individual strength values by the strength of a flat pillar of W/H ratio = 0.58. The strength of a 0° dipping pillar of W/H ratio = 0.58 is 21 MPa for 80 MPa intact strength, while it is 39.5 MPa for 150 MPa intact rock strength. The nonlinear response for normalized pillar strength illustrated in Figure 6 can be attributed to (1) the utilization of a nonlinear material model [7] and (2) the utilization of an interface at the roofline.

As illustrated in Figure 6, the modeled pillar strength increases with increasing its W/H ratio, and it decreases with increasing the seam inclination. When the seam inclination changes from 0° to 10°, the maximum reduction in modeled pillar strength is about 6% among all W/H ratios, and when the seam inclination changes from 0° to 20°, the maximum reduction in modeled pillar strength is about 16% among all W/H ratios. The impact of seam inclination on limestone pillar strength should not be ignored, particularly for 20° dipping pillars, especially when the W/H ratio is less than 1.0, for the following reasons: (1) there is a substantial reduction in pillar strength for a 20° dip angle for pillars of small W/H ratios, and (2) pillars of small W/H ratios are more sensitive to the existence of geological features, such as discontinuities, than pillars of larger W/H ratio, where the impact of discontinuities on dipping pillars could be higher than that for flat pillars.

Among the most important parameters that control the impact of seam inclination on pillar strength is the shear strength between the pillar and the roof. A strong interface between a stone pillar and the roof would produce a clamping effect and provide more lateral constraints, which provides the pillar with a supplemental strength and precludes the fracture propagation, hence further strengthening the pillar. A lower level of interface friction would allow slip and separation that would result in induced tensile stresses in the pillar. Figure 7 illustrates the variation of the normalized axial pillar strength with seam inclination for a strong roof/pillar interface; the intact rock strength for these models is 150 MPa. Hence, Figure 7 could be compared with Figure 6b to show that the effect of seam inclination on pillar strength becomes insignificant for a-type pillars when a strong interface—that does not allow sliding or separation—exists between pillars of the surrounding rock.

For the b-type pillars, the interface between the pillars and the surrounding rock is strong; consequently, the impact of seam inclination was insignificant on pillar strength when the dip angle was 20° or less like a-type pillars. However, the seam inclination started to influence pillar strength for 30° and 40° dip angles as illustrated in Figure 8 such that pillar strength decreases with increasing the dip angle. When seam inclination changes from 0° to 30°, the maximum reduction in pillar strength is 10% among all W/H ratios when the intact rock strength was 80 MPa, while it is 3% when the intact rock strength was 150 MPa. When seam inclination changes from 0° to 40°, the maximum reduction in pillar strength is 14% among all W/H ratios when the intact rock strength was 80 MPa while it is 11% when the intact rock strength was 150 MPa. Consequently, seam inclination should not be ignored for the b-type pillar even if there is a strong contact between pillars and the surrounding rock when the dip angle is greater than 20°.

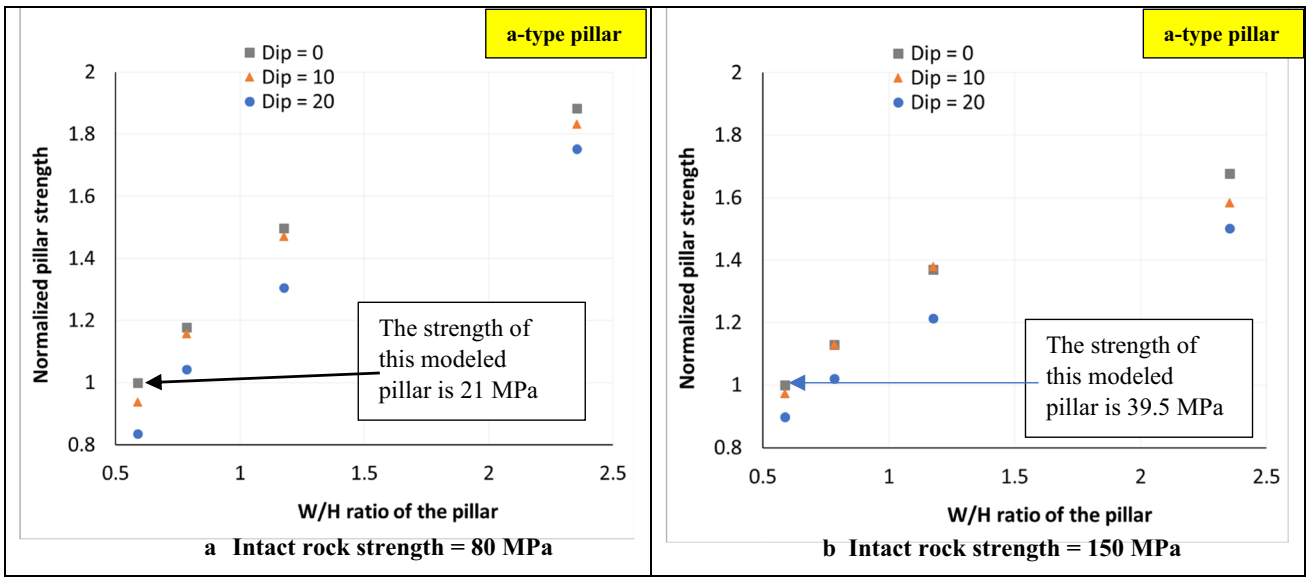

Fig. 6 Average pillar strength from FLAC3D models for the a-type pillar with weak roof/pillar interface; *k*-ratio = 3.0

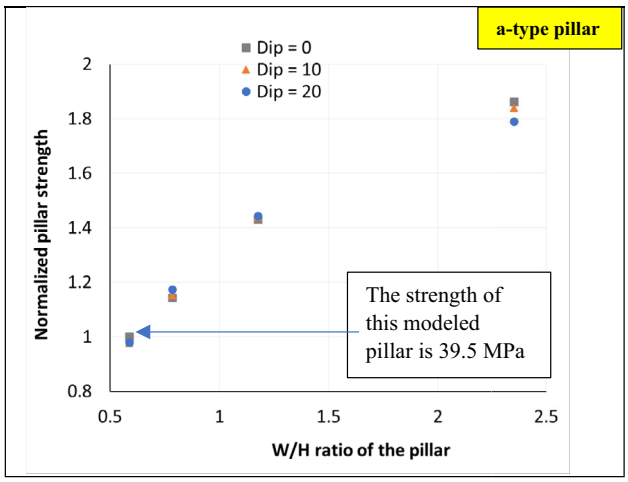

Figure 7 Average pillar strength from FLAC3D models for the a-type pillar with strong roof/pillar interface; *k*-ratio = 3.0 and UCS = 150 MPa

9 Dipping Pillars Are at an Elevated Risk of Instability

To evaluate dipping pillar stability when the W/H ratio of the pillar is small (≤ 1.0), it is not recommended to solely depend on an average safety factor at mid-height of the pillar because the safety factor might be significantly low at a specific direction that is different from mid-pillar height. Figure 9 shows the zone strength-stress ratio (SSR) at mid-pillar height for the a-type pillar and a flat pillar of the same W/H ratio, the *k*-ratio =3. Similar patterns were observed in *k*-ratio = 0.3 for weak or strong interface conditions. The SSR is the safety factor for elements based on shear failure; it does not consider any potential tensile failure. As illustrated in Figure 9, for the a-type pillar, the lowest SSR occurs along the short diagonal—not mid-height of the pillar—with an average value of 1.85, while it is about 3.11 when it was estimated at mid-height of the pillar. A similar pattern was observed for the b-type pillars. On the other hand, for flat pillars, the most critical location to estimate the safety factor is at mid-pillar height. Hence, to properly evaluate pillar stability in underground limestone mines from numerical models, it is important to recognize the critical path where the expected safety factor would be minimum.

Hedley 6 recognized that seam inclination is one of the main factors that can contribute to rock-burst. The oblique loading path generated from seam inclination may place the a-type and b-type pillars at an elevated risk of instability for many reasons: (1) The shear stress is higher along the oblique loading path compared to the axial loading path in flat pillars (see Figure 10) which shows the maximum shear stress distribution for the a-type pillar and a flat pillar of the same W/H ratio. Flat pillars of a small W/H ratio experience more uniform stress distribution [20]. However, in the case of dipping pillars, they experience non-uniform stress distributions (stress gradient) that vary rapidly with position as illustrated in Figure 10a. A similar pattern was observed for the b-type pillars.

(2) Dipping pillars experience less confinement compared to flat pillars. Figure 11 shows the variation of the minimum principal stress (σ_3) with the W/H ratio at various dip angles for the a-type and b-type pillars. The minimum principal

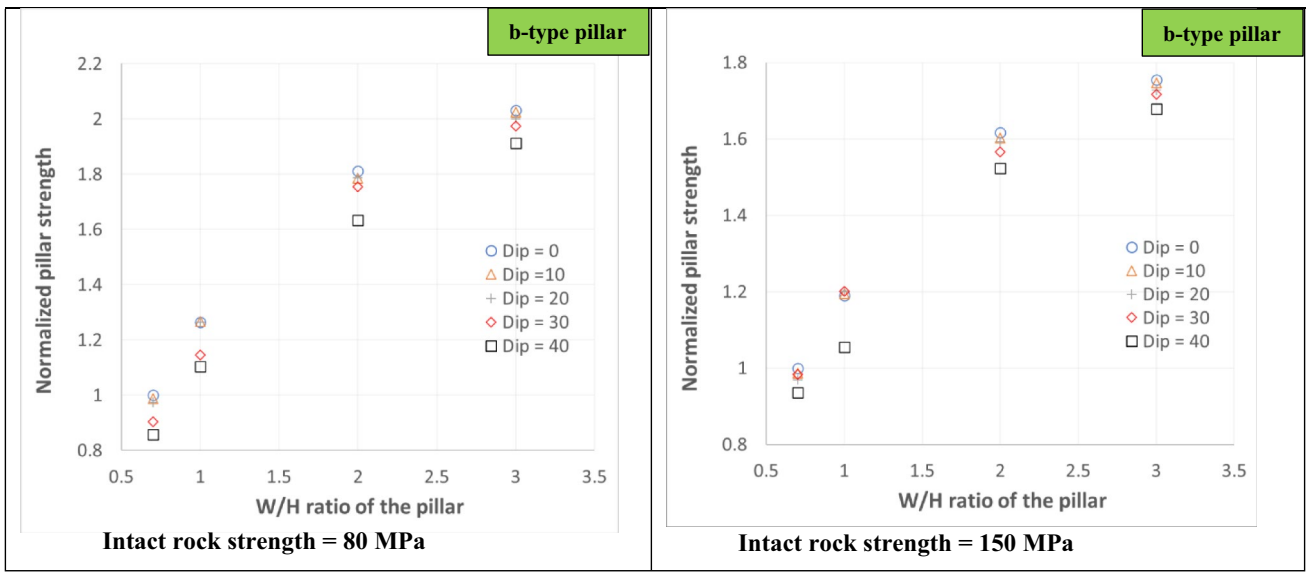

Fig. 8 Average pillar strength from FLAC3D models for the b-type pillar with strong roof/pillar interface; *k*-ratio = 3.0. The pillars have a square projected cross-sectional area

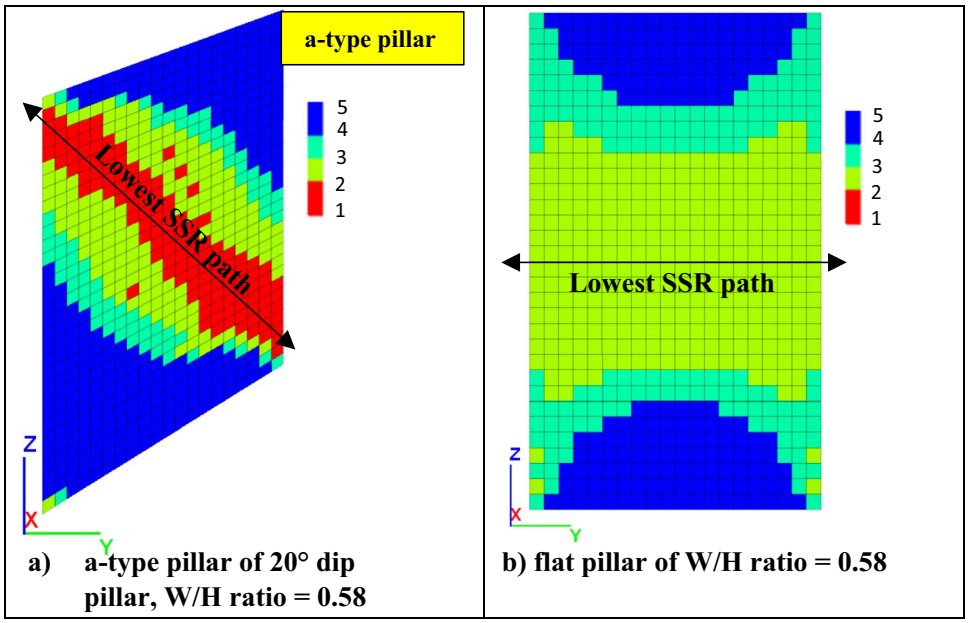

Fig. 9 Strength-stress ratio (SSR) for the a-type pillar and flat pillar with weak interfaces at the development loading stage; the UCS = 150 MPa and the *k*-ratio = 3.0

stress—the confinement—increases with increasing the W/H ratio of the pillar, and it decreases with increasing the seam inclination. The impact of seam inclination on the confinement is higher for pillars having bigger W/H ratios. The amount of dilation is expected to be higher for dipping pillars compared to flat pillars since the dilation decreases with increasing confinement.

(3) The yielding due to loading is greater for dipping pillars than that of flat pillars, and it increases generally as the dip angle increases. Figure 12 illustrates the variation of percent yield for the a-type pillars of W/H ratio = 0.58 and weak roof interface and the b-type pillars of W/H ratio = 0.70. Previous research reached similar findings [26], [14], [28].

10 Effect of Dip on Rib Deformation from Numerical Models

Seam inclination can cause not only a major effect on the magnitude and orientation of the induced stresses, but also it creates an uneven deformation at the up-dip and down-dip sides of the pillar, such that the magnitudes of vertical and outward-horizontal displacements at these opposite sides are uneven. The displacement magnitude can be used as a proxy for damage or a tool to show relatively where to expect a problem as these opposite sides are uneven. It is more likely to observe more pillar deterioration in areas with high displacement. Figure 13 illustrates the change in the vertical

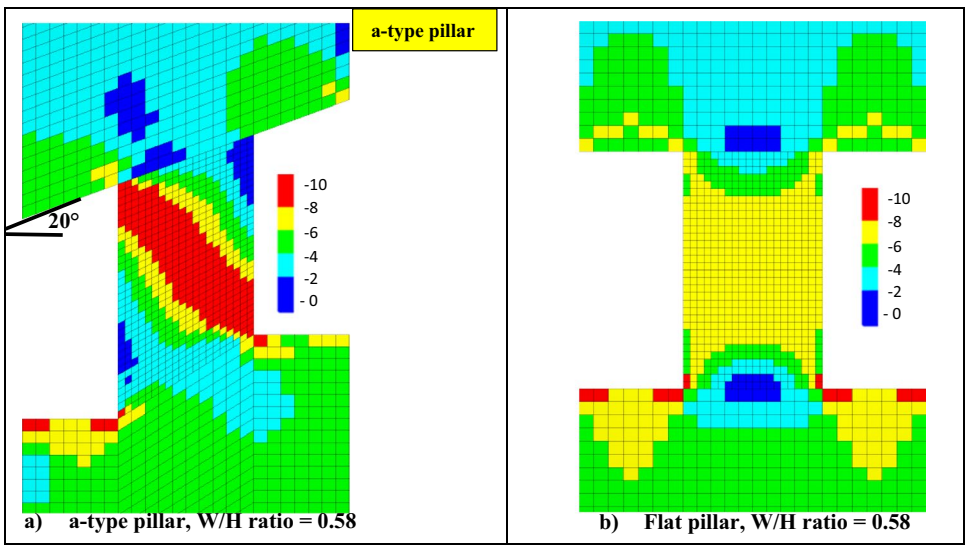

Fig. 10 Maximum shear stress distribution for the a-type pillar of 20° dip and a flat pillar with weak interfaces at the development loading stage; UCS = 150 MPa; *k*-ratio = 3.0. Units are in MPa. Negative values mean compression

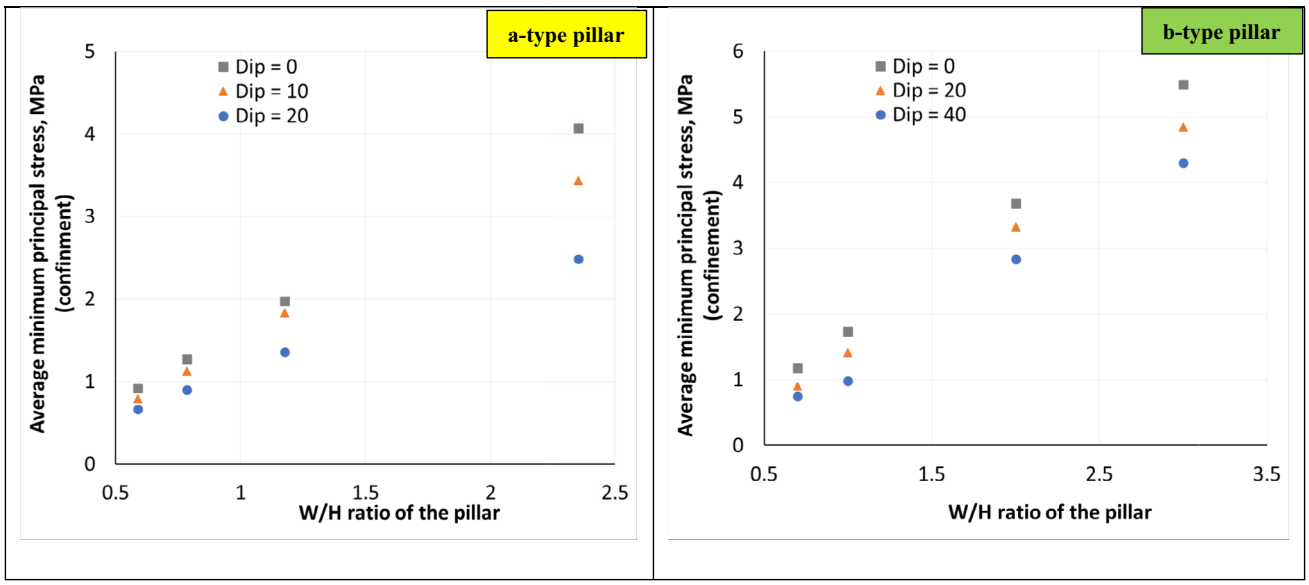

Fig. 11 Variation of the average minimum principal stress with W/H ratio at different dip angles for a-type and b-type pillars at the development loading stage

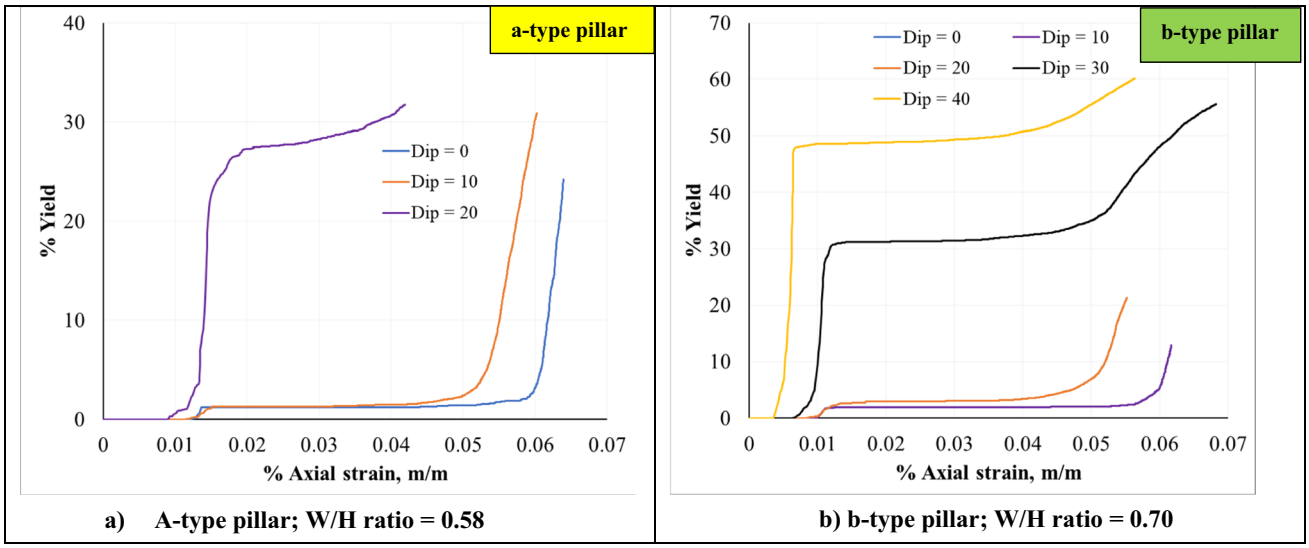

Fig. 12 %yield for the a-type and b-type pillars at various dip angles. The UCS = 150 MPa and the *k*-ratio = 3.0

displacement (Z-displacement) for up- and down-dip sides of the a-type pillar having a 20° dip angle and a flat pillar of the same W/H ratio. The magnitude of the vertical displacement for a pillar side is estimated by averaging the Z-displacements for all grid points composing that side. For a flat pillar, the vertical displacement is identical at the two opposite sides, which is why the vertical displacement at only one side is illustrated in Figure 13. However, for a dip pillar, the up-dip (short) side of the pillar experienced more vertical displacement than the down-dip (tall) side. Similar trends were found for b-type pillars.

The horizontal displacement could produce a crack opening in a brittle rock-like limestone material since the tensile strength of rock is significantly lower than the compressive strength. The impact of seam inclination on the outward normal displacement for dipping pillars could be more pronounced if a jointed material model was used rather than the isotropic Hoek-Brown material model used in this study. It should also be mentioned that the horizontal displacement is lower than the vertical displacement for pillar sides based on the numerical model results. For the a-type pillars at the development loading stage, the tall side (down-dip side) of the pillar experienced more horizontal

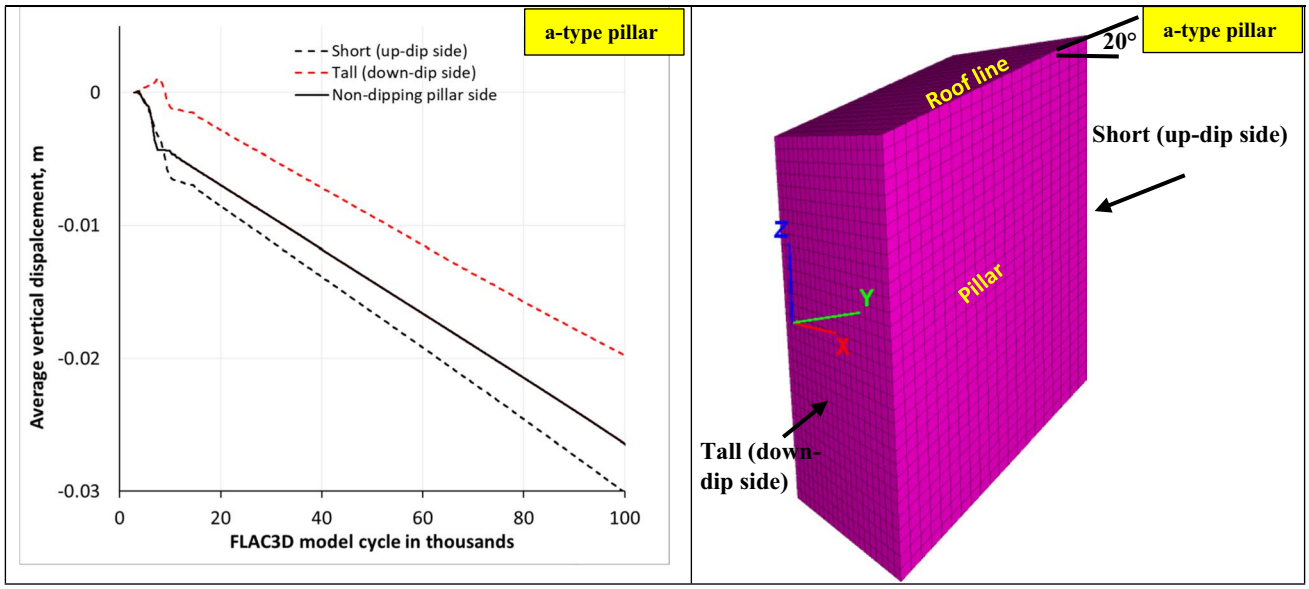

Fig. 13 Average vertical displacement for short and tall sides of the a-type pillar of 20° dip versus equivalent sides of a flat pillar of W/H ratio 0.58. UCS = 150 MPa; *k*-ratio = 3.0

displacement than the short side (up-dip side) of the pillar. However, the rate of change in the horizontal displacement for the up-dip side is higher than the down-dip side such that the short side of the pillar starts to see more horizontal displacement when the pillar is close to its ultimate strength; this behavior is illustrated in Figure 14, which illustrates the variation in the outward normal displacement (horizontal displacement/Y-displacement) for 20° dip and flat pillars of the a-type geometry. The magnitude of the horizontal displacement for a pillar side is estimated by averaging the Y-displacements for all grid points composing that side of the pillar.

11 Effect of Dip on Rib Deformation from LiDAR Scan

3D LiDAR scanning was conducted at a dipping mine with a-type pillar geometries and was used to map damage to pillars with varying W/H ratios. The results of the scanning yielded trends as to where damage was concentrated on the pillar. Often, sloughing would occur on the tall side of the pillar, and as W/H ratios decreased, the sloughing would become more pronounced. Prior to benching, the damage would begin on the tall side of the pillar, so that when benching occurred, the top half of the pillar would be more damaged than the bottom half. In Figure 15, damage can be found on the top portion of the tall side of the pillar, and exposed roof bolts in the top portion of the ribs in a benched area show the pillar's original dimension at those points. 3D LiDAR scans were collected over a wide area of the mine and generally showed that the damage concentrated on the tall side of the pillar, causing increased surface roughness and sloughing as shown in Figure 16 at two different locations in the mine.

12 Effect of Seam Inclination on Yield Pattern

For flat pillars, the yield pattern is simple and generally does not change with changing the strength, W/H ratio of the pillar, or in situ stress conditions. Usually, the yield pattern starts at the corners and the edges and propagates toward the pillar core. If the interface strength between the roof/pillar and the floor/pillar is equal, the yield pattern would be symmetric for both Z-Z and Y-Y axes as shown in Figure 17. However, differences in roof/pillar or pillar/floor interfaces may create vertical asymmetry. On the other hand, for dipping pillars, the yield pattern is more complicated. It depends on numerous parameters, such as the W/H ratio of the pillar, in situ stress conditions, the shear strength of the interface between the pillar and both roof and floor, the dip angle, and the geometry of the pillar. Simplifying a modeled pillar geometry in dip mines may introduce unrealistic rock failure responses and yield patterns [23]. For the a-type pillar, when the W/H ratio of the pillar is less than 1.0, the yield pattern goes through the short diagonal, and it propagates through the pillar core. Increasing the W/H ratio of a dipping pillar could change the yield pattern. For instance, having the same in situ stresses and interface conditions shown in Figure 18 but increasing the W/H ratio of the pillar would

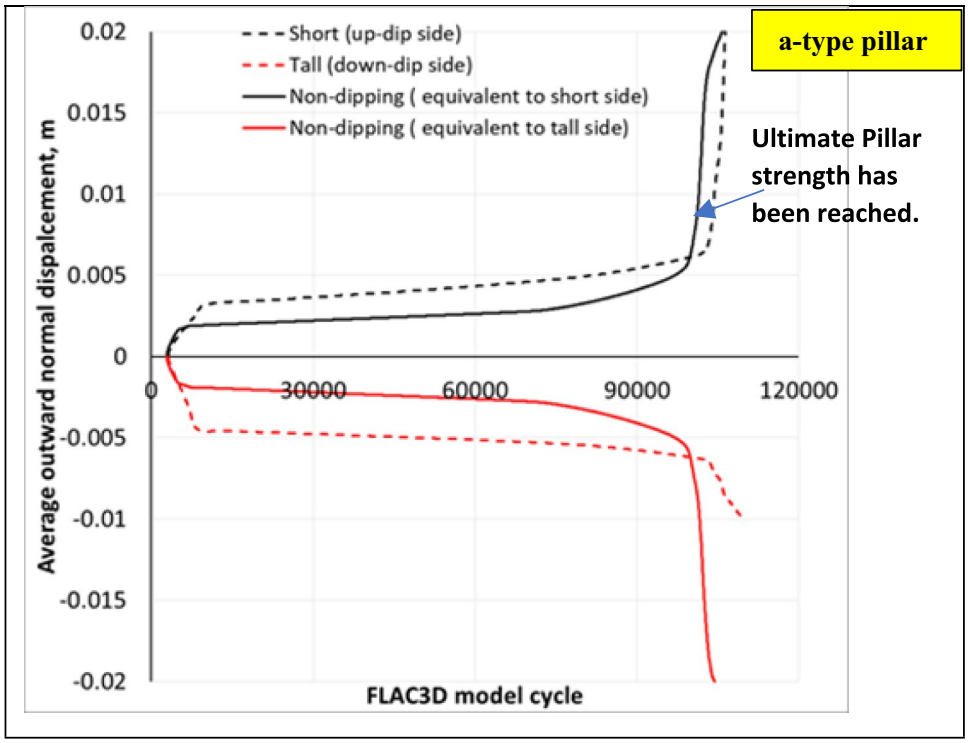

Fig. 14 Average outward normal displacement (Y-displacement) for short and tall sides of 20° dipping pillar versus equivalent sides of a flat pillar of W/H ratio 0.58. UCS = 150; *k*-ratio = 3.0

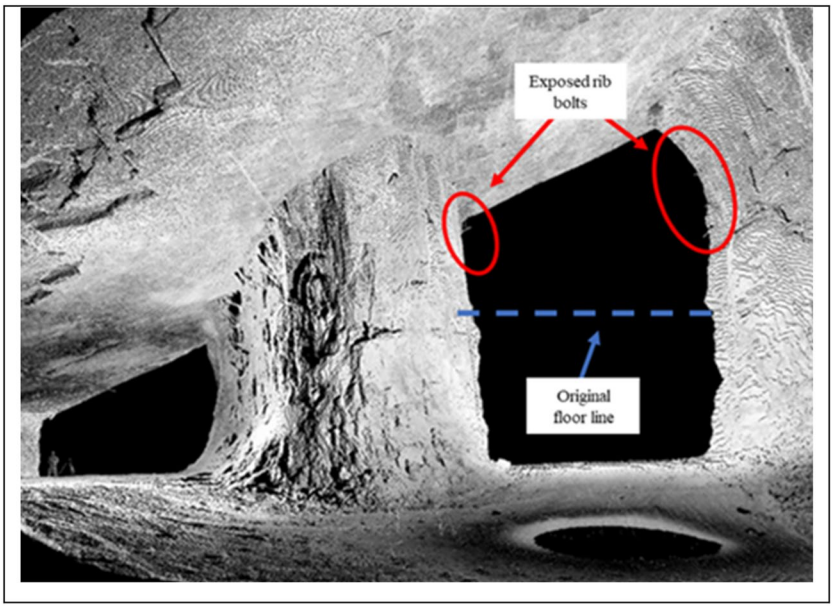

Fig. 15 3D LiDAR scan of damage to the top portion of ribs in a benched area of a dipping mine of a-type geometry

increase the strength of the core elements and hence prevent the yield pattern from propagating toward the pillar core.

13 Conclusion

This study shows how numerical models have been utilized to gain more insight about the impact of numerous factors on dipping pillar stability in underground limestone mines. Two actual mine geometries (a-type and b-type) have been used in this study because a simplified mine geometry could create an unrealistic failure propagation pattern and hence an inaccurate prediction for pillar strength. In a-type mine geometry, the roof is dipping while the floor is flat making one side of the pillar shorter than the other side. In b-type mine geometry, the roof and floor lines of pillars are dipping while the headings/crosscuts are flat. For the a-type geometry, the numerical models were

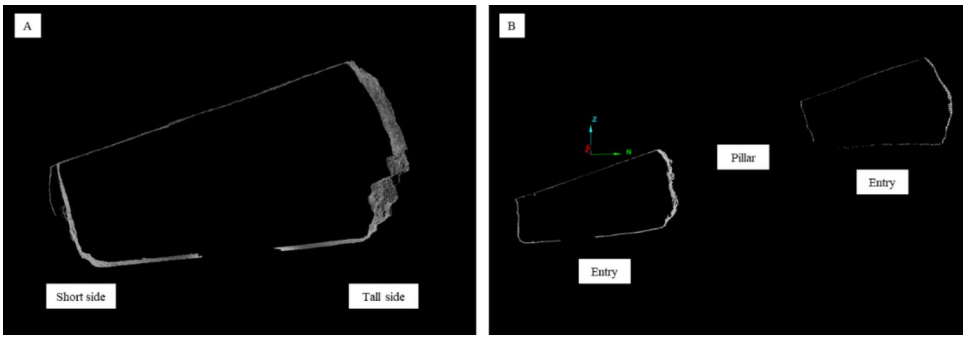

Fig. 16 3D LiDAR scan profiles of dipping pillars with increased damage on the tall side of the pillars at two different locations. The non-verticality of the ribs highlights the extent of damage

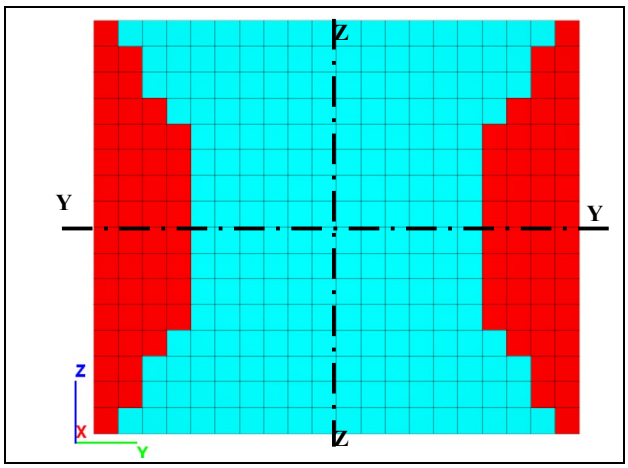

Fig. 17 Symmetric yield pattern for a flat pillar. Yielded elements are red and elastic elements are blue

generated with weak and strong interface conditions such that in strong interface conditions the pillar is attached to the surrounding rock. On the other hand, for the type-b geometry, only strong interface conditions were utilized.

For the a-type geometry and weak interface condition, the average pillar strength decreases with increasing the seam inclination, When the seam inclination is 10° or less, the effect of seam inclination on average pillar strength is insignificant; when the seam inclination is 20°, the maximum reduction in pillar strength is about 16% among all W/H ratios. A strong interface between pillars and surrounding rock produces a clamping effect and more lateral constraints that preclude the fracture propagation and hence strengthen the pillar, which is why the impact of dip became insignificant at a 20° dip angle when a strong interface was used; a similar pattern was found in the b-type geometry. However, when the dip angle is 30° or more, the seam inclination has an impact on average pillar strength.

Dipping pillars are at an elevated risk of instabilities particularly if the W/H ratio of the pillar is small (less than 1.0) because the induced stresses in dipping pillars are higher than the flat pillars. Additionally, the confinement (the minimum principal stresses) in the pillar decreases with increasing the seam inclination. Seam inclination creates a state of uneven deformation in the pillar such that the magnitudes

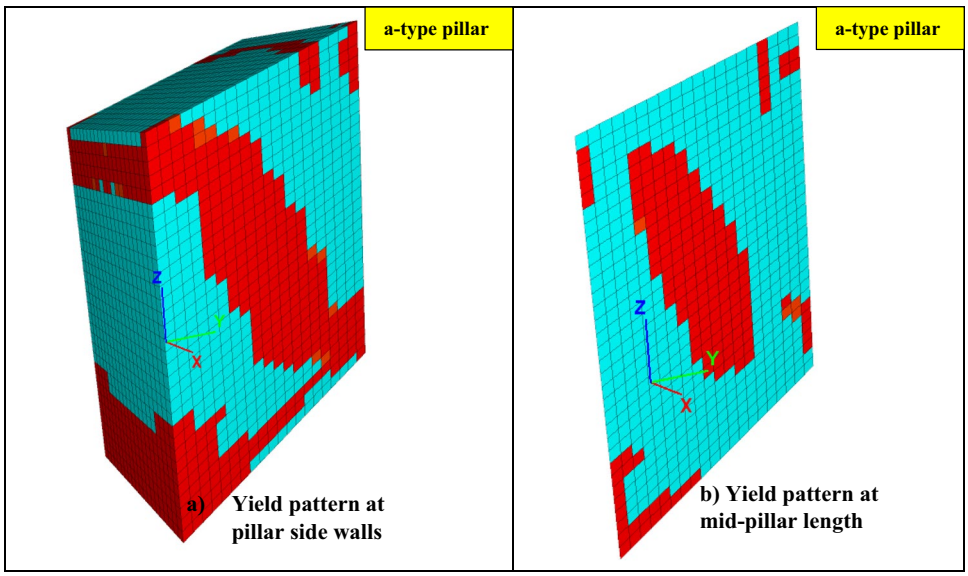

Fig. 18 Yield pattern for the a-type pillar of 20° dip angle and W/H ratio = 0.58 in a high horizontal stress field

of the vertical and horizontal deformation in the up-dip and down-dip sides of the pillar are not the same. Also, seam inclination creates an asymmetric loading path and yield pattern in the pillar; it is recommended to evaluate the stability of a dipping pillar of a small W/H ratio along the short diagonal, not along the mid-height of the pillar. The outcome of this provides some design considerations that could help reduce the potential of dipping pillar instability in underground limestone.

14 Limitations/Constraints of This Study

Stone pillar stability can be affected by many factors including the in situ stresses and geological discontinuities [9]. Additionally, weak bands and karst cavities in stone pillars can significantly reduce pillar strength. Weak bands can induce tension in the stronger rock slabs [3], while the karst cavities weaken the limestone pillars since limestone materials have been removed, and also, they act as water pipes to transmit water through the rock mass. Discontinuities, karst cavities, and weak bands driven by instabilities are not considered in this study because they are highly variable and site specific. The main purpose of this work is to study the response of dipping pillars to loading more generally so that it can be applied to situations where the impact of discontinuities or weak bands is well understood or insignificant. The quality of rock mass can also impact the strength of stone pillars. Only one rock mass quality with a geological strength index (GSI) of 75 was utilized in this study to simulate a moderate rock mass quality. The damage observed from the 3D LiDAR scans was based on visual assessment, and it does not include exact volume changes over time. Finally, the findings in this study are limited to the variables evaluated. While the authors did choose to evaluate variables based on common conditions from their experience, every permutation of pillar geometries and loading conditions cannot possibly be considered. The common situations and conditions considered here are to highlight potential areas of concern when evaluating or designing pillars in dipping environments.

Declarations

Disclaimer The findings and conclusions in this study are those of the authors and do not necessarily represent the official position of the National Institute for Occupational Safety and Health (NIOSH), the Centers for Disease Control and Prevention (CDC). Mention of any company or product does not constitute endorsement by NIOSH.

References

1. Brady BHG (1977) An analysis of rock behavior in an experimental stoping block at the Mount Isa Mine, Queensland, Australia. Int J Rock Mech Min Sci Geomech Abstr 14(2):59–66
2. Dougherty H, Slaker B, Murphy MM (2019) An industry survey: mining environment and ground control citations. In: Presentation at the 24th Annual Underground Stone Safety Seminar
3. Esterhuizen GS, Ellenberger JL (2007) Effects of weak bands on pillar stability in stone mines: field observations and numerical model assessment. Proceedings of the 26th International Conference on Ground Control in Mining, Morgantown, West Virginia. pp 320-326
4. Esterhuizen GS, Iannacchione AT (2005) Effect of the dip and excavation orientation on roof stability in moderately dipping stone mine workings. Alaska Rocks 2005, 40th U.S. Symp. Rock
5. Hedley DGF, Grant F (1972) Stope and pillar design for the Elliot Lake Uranium Mines. CIM Bull 65:37–44
6. Hedley DGF (1992) Rockburst handbook for ontario hardrock mines. CANMET Special Report SP92- 1E. Canada Communication Group, Ottawa, pp 23 1-242
7. Hoek E, Brown ET (2018) The Hoek-Brown failure criterion and GSI – 2018 edition. J Rock Mech Geotech Eng. https://doi.org/10.1016/j.jrmge.2018.08.00
8. Hoek E, Diederichs MS (2006) Empirical estimation of rock mass modulus. Int J Rock Mech Min Sci 43(2):203–2015
9. Iannacchione T (1999) Analysis of pillar design practices and techniques for U.S. limestone mines. Trans Inst Min Metall (sect. A:Min. Industry) 108:A152–A160
10. Itasca Consulting Group (2018) "Fast Lagrangian analysis of Continua in 3 dimensions"; Itasca Consulting Group: Minneapolis. MN, USA
11. Jaeger JC, Cook NGW, Zimmerman RW (2007) Fundamental of rock mechanics, 4th edn. Blackwell Publishing
12. Jessu KV, Spearing AJS (2018) Effect of dip on pillar strength. J South African Inst Min Metall 118:765–776
13. Krauland N, Soder PE (1987) Determining Pillar strength from pillar failure observation. E&MJ-Eng Min J 188(8):34–40
14. Kvapil RL, Beaza JR, Flores G (1989) Block caving at EI Teniente Mine, Chile". Inst Min Metall 98(6):A43–A56
15. Lorig LJ, Cabrera A (2013) Pillar strength estimates for foliated and inclined pillars in schistose material. In: Zhu H et al (ed) Continuum and Distinct Element Numerical Modeling in Geomechanics. (CD Proceedings, 3rd International FLAC/DEM Symposium, Hangzhou, China, October 2013). Paper: 01-01. Minneapolis: Itasca International, Inc.
16. Lunder PJ, Pakalnis RC (1997) Determination of the strength of hard-rock mine pillars. Bull Can Inst Min Metall 90(1013):51–55
17. Martin CD, Maybee WG (2000) The strength of hard rock pillars. Int J Rock Mech Min Sci 37:1239–1246
18. MSHA data retrieval system (2023) Mine Data Retrieval System | Mine Safety and Health Administration (MSHA)
19. Murphy M, Slaker B, Iannacchione A, Rashed G, Buchan G, Van Dyke M, Minoski T, McElhinney D, Winfield J (2018) Development of a comprehensive pillar and roof monitoring system at a steeply dipping underground limestone mine. In: 2018 SME Annual Meeting and Exhibit
20. Obert L, Duvall W (1967) Rock mechanics and the design of structures in rock. John Willey & Sons Inc

21. Pariseau WG (1982) Shear stability of mine pillars in dipping seams. 23rd U.S. Symposium on Rock Mechanics (USRMS). Berkeley, California
22. Pritchard C, Hedley D (1993) Progressive pillar failure and rockbursting at denison mine. In: Balkema AA (eds) Proceedings of 3rd International Symposium on Rockbursts and Seismicity in Mines, Kingston. Rotterdam, p 111 J6
23. Rashed G, Slaker B, Sears MM, Murphy MM (2021) A parametric study for the effect of dip on stone mine pillar stability using a simplified model geometry. Min Metall Explor 38:967–977. https://doi.org/10.1007/s42461-021-00394-y
24. Salmon MDG, Munro AH (1967) A study of the strength of coal pillars. South Afr Inst Min Metall 68:55–67
25. Sjöberg J (1992) Failure modes and pillar behavior in the Zinkgruvan Mine. In: 33rd U.S. Symposium on Rock Mechanics. USRMS, pp 491–500
26 Suorineni FT, Mgumbwa JJ, Kaiser PK, Thibodeau D (2011) Mining of orebodies under shear loading. Part 1 – case histories. Trans Inst Min Metall Sect A: Min Technol 120(3):138–147
27. Von Kimmelmann MR, Hyde B, Madgwick RJ (1984) The use of computer applications at BCL limited in planning pillar extraction and the design of mining layouts. Design and Performance of Underground Excavations. ISRM/BGS, Cambridge, pp, 53-63
28. Whyatt J, Varley F (2008) Catastrophic failures of underground evaporite mines. Proc. 27th Intl. Conf. on Ground Control in Mining, Morgantown, WV, pp 113–122